Capillarity

Vol. 19, No. 1, p. 15-25, 2026

Original article

Influence of fractal surface roughness on nanoparticle fluids driven spontaneous imbibition and enhanced oil recovery: A microfluidic study

Jiangtao Zheng[1,2], Tian Tian[2], Xianzheng Bao[2], Wenbo Gong[3], Jianchao Cai[4], Wenhai Lei[5]*

[1]*State Key Laboratory for Fine Exploration and Intelligent Development of Coal Resources, China University of Mining and Technology, Beijing 100083, P. R. China*

[2]*School of Mechanics and Civil Engineering, China University of Mining and Technology, Beijing 100083, P. R. China*

[3]*College of Safety and Ocean Engineering, China University of Petroleum, Beijing 102249, P. R. China*

[4]*State Key Laboratory of Petroleum Resources and Engineering, China University of Petroleum, Beijing 102249, P. R. China*

[5]*Manchester Centre for Nonlinear Dynamics, Department of Physics and Astronomy, University of Manchester, Manchester M13 9PL, UK*

Keywords:
Pore-scale
surface roughness
nanoparticle fluids
precursor wetting film

Cited as:
Zheng, J., Tian, T., Bao, X., Gong, W., Cai, J., Lei, W. Influence of fractal surface roughness on nanoparticle fluids driven spontaneous imbibition and enhanced oil recovery: A microfluidic study. Capillarity, 2026, 19(1): 15-25.
https://doi.org/10.46690/capi.2026.04.02

Abstract:
Although nanoparticle fluids outperform conventional surfactants in spontaneous imbibition related oil recovery, the specific role of pore surface roughness remains elusive. This study investigates the impact of fractal roughness on spontaneous imbibition-driven displacement through microfluidic experiments, utilizing Koch-curve-based channels of varying geometric complexity. By tracking main meniscus retreat and analyzing corner or film flow, we quantitatively compare the oil recovery efficiency of nanoparticle fluid versus surfactant solution. Experimental results demonstrate that nanoparticle fluid consistently outperformed surfactant solution in oil recovery, with this advantage becoming more pronounced as surface roughness increases. Visualization reveals that nanoparticles promote oil detachment by accelerating corner flow and facilitating wetting-film propagation along rough walls. Based on these insights, a roughness-informed analytical framework is developed to predict nanoparticle fluid enhanced recovery. This work provides pore-scale insights and a theoretical framework for evaluating nanoparticle fluid-enhanced oil recovery strategies in rough and heterogeneous unconventional reservoirs.

1. Introduction

Nanoparticle fluids (NFs) exhibit unique interfacial regulation mechanisms during spontaneous imbibition (SI), leading to significant improvements in both sweep efficiency and oil displacement efficiency (Alvarez-Berrios et al., 2018; Nguele et al., 2019; Yarveicy, 2023; Jing et al., 2025). SI plays a critical role in enhanced oil recovery (EOR), particularly in low-permeability unconventional reservoirs. In such systems, external pressure gradients are limited, and fluid mobilization is predominantly governed by capillary forces (Hu et al., 2020; Tian et al., 2021; Zheng et al., 2024). Extensive experimental and theoretical studies have demonstrated that the interfacial dynamics of nanoparticle suspensions play a key role in SI (Youssif et al., 2018; Tavakkoli et al., 2022). Specifically, suspended nanoparticles can adsorb at fluid-solid and fluid-fluid interfaces, thereby reducing interfacial tension

Yandy Scientific Press

*Corresponding author.
E-mail address: zhengjt@cumtb.edu.cn (J. Zheng); tiant0206@163.com (T. Tian); 15005656942@163.com (X. Bao); wenbog@cup.edu.cn (W. Gong); caijc@cup.edu.cn (J. Cai); leiwenhai12@gmail.com (W. Lei).

Received January 26, 2026; revised February 25, 2026; accepted March 13, 2026; available online March 16, 2026.

and altering wettability (Kondiparty et al., 2011; Lim et al., 2016; Lei et al., 2023; Furedi et al., 2024). In comparison, surfactant flooding can also enhance oil mobilization through interfacial tension reduction and wettability modification (Guo et al., 2005; Belhaj et al., 2019). However, its overall EOR performance is often inferior to that of nanoparticle fluid systems (Ko and Huh, 2019; Sekoai et al., 2019; Yekeen et al., 2019). Therefore, systematic comparisons between NFs and surfactant solutions are essential. A deeper understanding of the governing interfacial dynamics is also required to elucidate the mechanisms underlying the superior performance of NFs (Robbins et al., 1991; Murshed and Nieto de Castro, 2011; Anand et al., 2021).

The pore structure of reservoir rocks exhibits pronounced geometric complexity, characterized by irregular pore shapes and rough surfaces (Burstein, 2011; Panter et al., 2023; Wang et al., 2023; Lei et al., 2024). Such geometric complexity promotes the development of corner flow and thin-film flow. The wetting phase spreads along pore corners and rough walls, thereby facilitating oil detachment (Ruiz-Gutiérrez et al., 2022; Zhao et al., 2022; Cardona and Santamarina, 2023). However, these geometric features can also exert adverse effects. Variations in surface roughness and curvature alter local film thickness and interfacial curvature. This redistributes capillary forces and affects film stability (Thiele et al., 2009; Geistlinger et al., 2015). Previous studies have shown that pore surface roughness introduces multiscale geometric undulations. These act as a primary trigger for film instability and rupture (Robbins et al., 1991; Ajaev et al., 2016). In particular, liquid films are more prone to drainage, thinning, and eventual breakup in protruding regions (MacDowell et al., 2014). As a result, enhancing film flow while maintaining film stability in complex pore geometries remains a central challenge for improving displacement efficiency during SI.

Recent studies suggest that NFs can form multiscale structures on complex pore surfaces, thereby enhancing the stability of wetting films (Li et al., 2020). Our previous work demonstrated that nanoparticle adsorption on pore walls induces nanoscale structures. Combined with microscale pore geometries containing dead-end features, these structures form a multiscale system and generate a stable, continuous nanoparticle-induced wetting film (Lei et al., 2025). During displacement, this nanoparticle-induced wetting film remains continuous and is driven by capillary pressure gradients. This promotes the release of non-wetting fluids trapped in dead-end structures and significantly enhances displacement efficiency (Zhang et al., 2018; Ratanpara and Kim, 2023; Lu et al., 2026). In contrast, conventional surfactant systems fail to establish such multiscale structures and are therefore more prone to film rupture under rough pore surface conditions. Despite growing recognition of the relationship between film stability and surface roughness, a systematic understanding remains lacking. The role of nanoparticle-induced multiscale structures in maintaining connected precursor wetting films is also not fully understood (Kovalchuk et al., 2014). In particular, direct pore-scale visualization and quantitative characterization of these processes in rough porous media are still limited.

In this study, a microfluidic experimental platform was employed to visualize SI in flow channels with controlled surface roughness. Fractal roughness structures were constructed based on Koch curves, representing three levels of geometric complexity. The interfacial dynamics under controlled roughness conditions were systematically investigated. First, NFs and surfactant systems with comparable interfacial tension and contact angle were prepared for direct comparison. During the visualization experiments, the retreat of the main meniscus was monitored to characterize corner flow and precursor wetting film formation. Meniscus retreat was compared at fixed time intervals across models with different roughness levels. This approach enables analysis of how pore surface roughness governs NF migration during SI. The results demonstrate the superior displacement performance of NFs over surfactant solutions. They also provide a quantitative experimental framework for evaluating NF-based EOR strategies in rough and heterogeneous unconventional reservoirs.

2. Experimental methods

2.1 Design of micromodels

To systematically investigate the effect of surface roughness on the oil recovery efficiency of NFs, microfluidic chips with different roughness characteristics were designed and fabricated (Fig. 1). Two buffer zones were incorporated adjacent to the inlet and outlet, as shown in Fig. 1(a). The observation region was located in the central part of the model, focusing on SI within flow channels with rough surfaces. All micromodels shared identical channel depth and width, with a channel depth of $H = 20$ μm and a main channel width $W = 300$ μm. The fractal roughness structures were confined to the observation region, where three parallel roughened channels were constructed, each with a length of $L = 6{,}750$ μm.

Surface roughness was constructed based on the fractal Koch curve, enabling systematic modulation of surface irregularity with high geometric reproducibility. Following the construction procedure, three models with different roughness levels were generated. The roughness was quantitatively defined as the ratio of actual length to projected length. The level 0 fractal structure corresponds to a smooth straight channel, as shown in Fig. 1(b), with a roughness of $R_n^0 = 1$. In the level 1 fractal structure, equilateral triangular elements were introduced along the channel walls, with a characteristic edge length of $a_1 = 150$ μm, as shown in Fig. 1(c), resulting in a roughness of $R_n^1 = 1.33$. In the level 2 fractal structure, additional triangular elements were introduced based on the level 1 geometry, with a reduced characteristic edge length of $a_2 = 50$ μm, yielding a roughness of $R_n^2 = 1.78$. Across the different rough structures, the channel surface evolves from smooth to increasing roughness.

The micromodels were fabricated using standard photolithography and wet etching techniques. Glass substrates were sequentially cleaned with organic solvents and deionized water, followed by nitrogen drying and thermal treatment. Microchannel patterns were defined by photolithography, and the exposed glass regions were etched using hydrofluoric acid to form the microchannels. Inlet and outlet reservoirs were created by precision drilling. The etched substrate was then

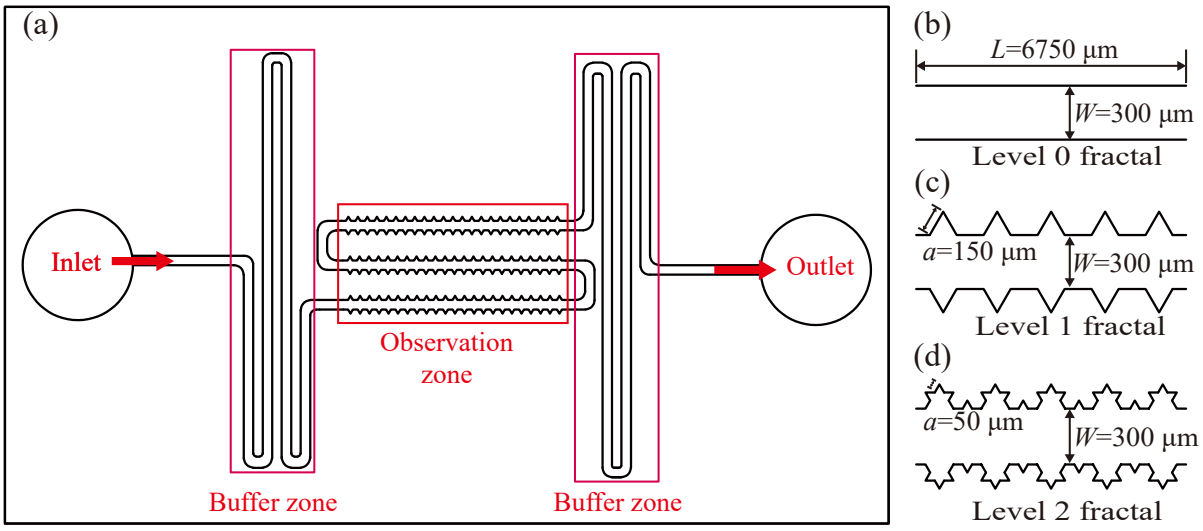

Fig. 1. Designed models incorporating fractal wall roughness: (a) Schematic representation of the model; (b)-(d) detailed views of fractal structures at levels 0, 1, and 2, respectively.

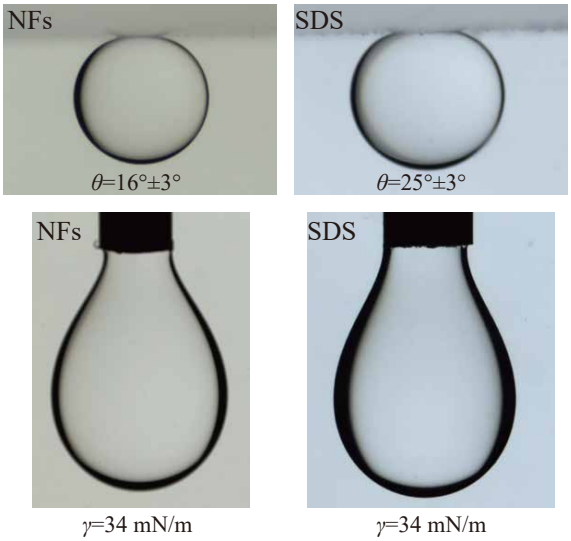

Fig. 2. Contact angle and surface tension of NFs and SDS surfactant solutions.

aligned with a glass cover plate and thermally bonded at elevated temperature, followed by slow cooling to room temperature to minimize thermal stress and obtain sealed micromodels (Whitesides, 2006; Song et al., 2014; Zhang et al., 2020).

2.2 Experimental fluids

Two displacement fluid systems were prepared for the visualization experiments. To ensure comparability, both systems were adjusted to have identical pH conditions and similar interfacial tension (Fig. 2).

For the NFs displacement system, n-decane (99%, Macklin) was used as the non-wetting phase, while a 5 wt% silica (SiO_2) nanoparticle suspension served as the wetting phase. The nanoparticles had an average diameter of 10 nm, and the system pH was 7. The interfacial tension between the NF and n-decane was $\sigma = 34$ mN/m, and the contact angle between the aqueous phase and oil on the glass surface was $\theta = 16° \pm 3°$.

For the surfactant system, sodium dodecyl sulfate (SDS) was dissolved in deionized water to prepare a 0.0015 wt% solution as the wetting phase, while n-decane served as the non-wetting phase. The system pH was 7. The interfacial tension was $\sigma = 33$ mN/m, which is comparable to that of NFs. The contact angle between the aqueous phase and oil was $\theta = 25° \pm 3°$.

Both displacement systems exhibited viscosities approximately equal to that of water ($\mu_w = 1.01$ mPa·s), as the low additive concentrations did not significantly alter the fluid viscosity. In addition, the contact angles were smaller than 45°. Under such wetting conditions, interfacial mechanisms, including corner flow and thin-film flow, dominate the displacement process.

2.3 Experimental procedures

Based on a self-designed transparent pore-scale experimental platform (Fig. 3), the evolution of two fluid systems in rough-surface channels was quantitatively characterized. The platform consists of three main components: A fluid injection system, a microscopic imaging system, and an image processing and analysis system. Fluid injection was controlled using a high-precision syringe pump (Harvard PUMP 11 PICO Plus Elite) and a precision syringe (HAMILTON 1705), ensuring a stable flow rate. The imaging system comprised a stereomicroscope (Leica M205 FCA) coupled with a CMOS camera (Leica K5C). This setup enables high-resolution visualization of pore-scale flow and interface evolution. Image processing and analysis were performed on a GPU workstation (NVIDIA Quadro RTX 8000) for efficient quantitative analysis of the acquired image sequences.

During the experiment, the chip was positioned under the

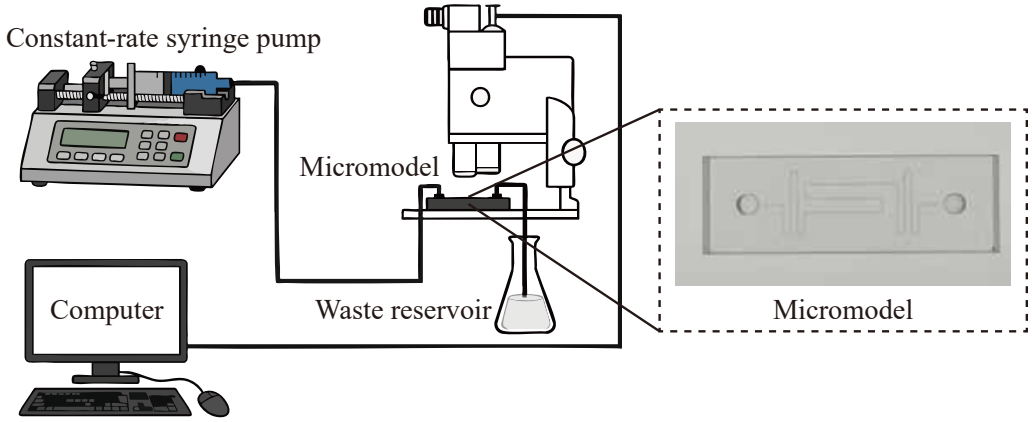

Fig. 3. Experimental platform with the micromodel enlarged.

objective of the stereomicroscope. The evolution of the two-phase interface was recorded by the imaging system, and the acquired images were transferred to a workstation for quantitative analysis.

The experimental procedures are as follows:

1) Three pore volumes of non-wetting phase were injected into the micromodel until the micromodel was fully saturated with oil.
2) Micromodels with different roughness levels were selected in the experiments. The NFs and the surfactant solutions were injected separately into the models at a constant rate of 3 nL/min, corresponding to a capillary number of $\mathrm{Ca} = 2.5 \times 10^{-7}$. Injection was terminated when the displacement front reached a predefined position within the rough channel. The inlet and outlet were then immediately sealed to establish a closed system.
3) Under sealed conditions, the evolution of the two-phase interface and the detachment of the oil during the SI process were recorded in real time. Each experiment lasted for 1 h.
4) The acquired image sequences were post-processed for quantitative analysis. The retreat of the main meniscus was extracted to characterize corner flow and thin-film flow.

In addition, detachment of the non-wetting phase was quantified. The interfacial dynamics of NFs and SDS surfactant solutions during SI were systematically compared.

All experiments were conducted under ambient laboratory conditions (approximately atmospheric pressure and 25 °C). Each experiment was repeated at least three times to ensure reproducibility, and consistent trends were observed across all trials.

3. Results

To compare displacement efficiency between NFs and surfactant solutions, interfacial evolution was recorded at identical time intervals. Fig. 4 presents a representative time series of interface evolution. In each image, the left side corresponds to the NF phase, while the right side corresponds to the oil phase. From top to bottom, the images show interface positions in fractal models at 0, 20, 40, and 60 min, respectively.

Migration of NFs is strongly influenced by fractal surface roughness, as reflected by interface positions at different time points.

During displacement, NFs migrate along the channel walls primarily through corner flow and thin-film flow. Due to mass conservation, preferential wall migration causes retreat of the main oil-water interface, leading to significant differences in interface positions among models with different roughness levels at identical time points. In the level 0 fractal structure, the pore walls are smooth along the flow direction, and no additional capillary pressure gradient is induced by surface roughness. Consequently, interface migration is not enhanced by roughness effects. In the level 1 structure, the NF phase fills only a single triangular roughness unit within 60 min. In the level 2 fractal structure, two symmetric pentagram-shaped units are completely filled over the same period. These observations indicate that increasing surface roughness enhances both corner flow and thin-film flow, thereby promoting the mobilization of trapped oil.

To further elucidate the displacement advantages of NFs under different surface roughness conditions, controlled experiments were conducted using SDS surfactant solutions for comparison. Fig. 5 presents the interfacial evolution between the surfactant solution and oil at different time points in models with varying surface roughness. In each image, the left side corresponds to the surfactant solution, while the right side corresponds to n-decane. From top to bottom, the images show interface positions at 0, 20, 40, and 60 min, respectively, for different fractal structures.

During the SI of SDS surfactant solutions, corner flow also develops under water-wet conditions. The interfacial tensions of the two fluid systems are approximately equal. As shown in Fig. 5, the main meniscus retreats to some extent in all roughness models after 60 min. This suggests that the surfactant system can promote oil detachment from pore walls during SI. However, the magnitude of meniscus retreat is consistently smaller than that observed in the NF system, reflecting its comparatively weaker displacement performance.

Further comparison shows that, for both NFs and SDS systems, meniscus retreat varies with surface roughness. This

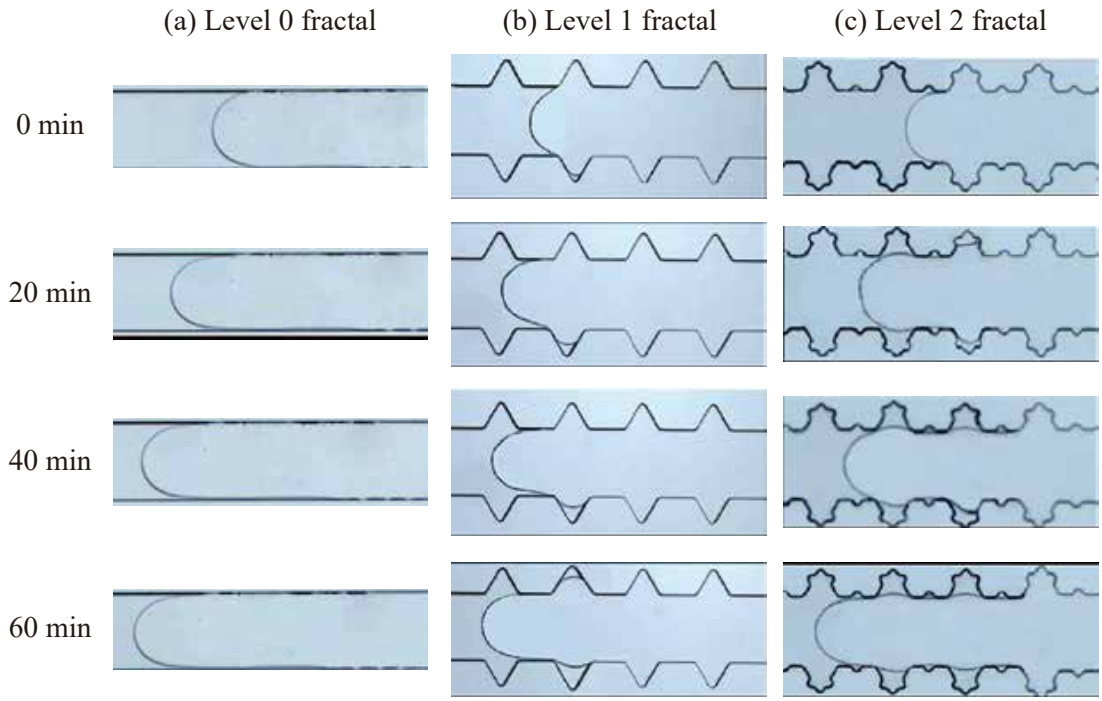

Fig. 4. Migration of the interface between the NFs phase and the oil phase at different time points: (a)-(c) Evolution of the fluid interface in the three different roughness models.

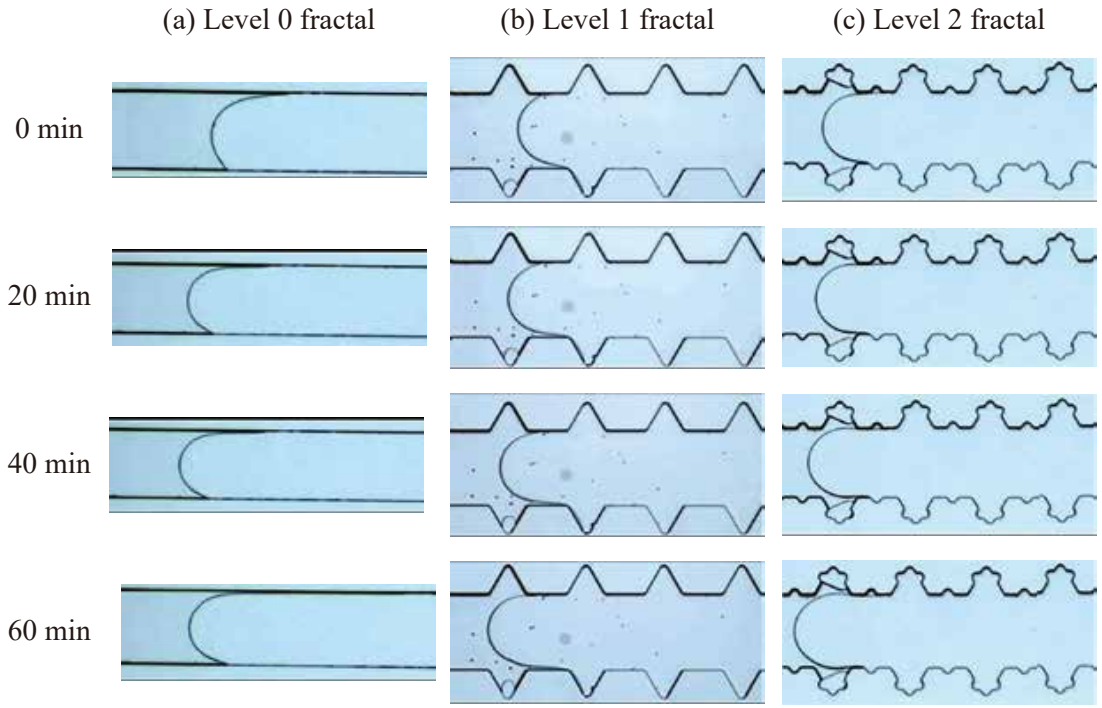

Fig. 5. Migration of the interface between the surfactant aqueous solution and the oil phase at different time points: (a)-(c) Evolution of the fluid interface for different fractal structures.

suggests that geometric effects influence the development of corner flow and thin-film flow. Notably, as surface roughness increases, the NF system exhibits a significantly greater enhancement in displacement efficiency than the surfactant system.

4. Discussion

Based on visualization experiments of SI in channels with different surface roughness, NFs consistently exhibit higher displacement efficiency than surfactant systems across all roughness levels. This section examines the underlying mechanisms from a pore-scale perspective. Furthermore, the oil volume released was quantified from the retreat of the main meniscus. This enables the oil recovery factor to be determined under different roughness conditions and allows systematic comparison of displacement performance.

4.1 NFs enhanced corner flow and thin-film flow

Surface roughness amplifies curvature gradients, thereby intensifying nanoscale film instability and nanoparticle-induced structural forces. Thin films are ubiquitous in multiphase flow within porous media, particularly near the three-phase contact line. Their formation, continuity, and stability critically govern fluid migration. As the film thickness decreases to the nanoscale, interfacial behavior can no longer be described solely by classical capillary pressure. Instead, disjoining pressure must be considered. Under such conditions, the pressure balance within the film region follows the augmented Young-Laplace equation (Nikolov et al., 2019; Lei et al., 2025):

$$P_c = \sigma\kappa + \Pi(h) \tag{1}$$

where P_c denotes the capillary pressure, σ is the interfacial tension, κ is the interfacial curvature, and Π is the disjoining pressure of the thin film. It depends on the film thickness h and can be determined using extended DLVO theory.

For NFs, particle aggregation and dispersion are governed by the effective interaction energy of the system. The total interaction energy can be expressed as (Matar et al., 2007; Lei et al., 2020; Xu et al., 2021):

$$W(h) = W_{VDW}(h) + W_{EDL}(h) + W_s(h) \tag{2}$$

where $W(h)$ denotes the total interaction free energy per unit area of the thin liquid film as a function of film thickness h. $W_{VDW}(h)$ represents the van der Waals attraction, $W_{EDL}(h)$ denotes the electrostatic double-layer repulsion, and $W_S(h)$ corresponds to the structural disjoining pressure arising from the confined arrangement of nanoparticles. These interactions can be quantitatively described using extended DLVO theory.

For the fluid systems considered in this study, the contact angle θ is smaller than 30°, favoring the formation of thin water films and corner flow. However, geometric constraints induced by surface roughness render these films susceptible to rupture, making film stability a key factor governing oil detachment efficiency.

Lei et al. (2025) demonstrated that thin-film stability in regions with varying surface curvature is governed by the competition between disjoining pressure and capillary pressure. When a critical curvature condition is satisfied, a molecular-scale adsorbed film transitions into a hydrodynamic film, forming a stable liquid film. The transition is governed by the range of disjoining pressure, characterized by $\Pi_{\max}$ and $\Pi_{\min}$. $\Pi_{\max}$ corresponds to the maximum repulsive interaction arising from electrostatic double-layer and structural forces, representing the upper limit at which a hydrodynamic film can resist capillary compression. $\Pi_{\min}$ denotes the minimum disjoining pressure dominated by attractive interactions, defining the lower bound below which capillary pressure can induce film thickening and trigger capillary condensation. These two characteristic values determine the transition between adsorption film and hydrodynamic film, as well as the conditions for film rupture and capillary condensation on multiscale surfaces. Under the present experimental conditions, the capillary pressure can be expressed as (Ichikawa et al., 2004):

$$P_c = 2\sigma\left(\frac{1}{W} + \frac{1}{H}\right) = 3.613 \text{ kPa} \tag{3}$$

where W is the main channel width (300 μm) and H is the depth (20 μm).

In convex curved regions, when $P_c > \sigma\kappa + \Pi_{\max}$, the disjoining pressure is insufficient to counterbalance the capillary pressure. Under this condition, the hydrodynamic film becomes unstable and ruptures, leaving only a stable molecular-scale adsorbed film.

In the present experiment, the convex surface curvature radius r_{cv} satisfies $r_{cv} < r_{cv,\,cri} = 1.26$ μm, where $r_{cv,\,cri}$ denotes the critical curvature radius below which the hydrodynamic film becomes unstable. This indicates that the curvature-induced capillary pressure exceeds the maximum attainable disjoining pressure. Consequently, only an adsorbed film remains stable in convex regions.

In the concave region, when $P_c < \sigma\kappa + \Pi_{\min}$ and the curvature radius satisfies $r_{cc} < r_{cc,\,cri}$, the capillary pressure is insufficient to suppress the structural disjoining pressure. The critical radius $r_{cc,\,cri} = 150$ nm corresponds to the onset of capillary condensation.

Under these conditions, capillary condensation is triggered, and the adsorbed molecular film transitions into a connected precursor wetting film (Tuller et al., 1999; Anand et al., 2021; Zhang et al., 2021).

Due to the continuous precursor wetting film network formed by nanoparticle adsorption on pore walls, the hydrodynamic wetting film generated in concave regions extends into adjacent convex regions. This leads to the transformation of the adsorbed film into a hydrodynamic wetting film, thereby enhancing overall film connectivity across rough surfaces.

In addition to nanoparticle-enhanced thin-film flow, corner flow plays a critical role in improving displacement efficiency. Due to the larger film thickness in corner regions, the associated disjoining pressure more readily satisfies the stability criterion. As a result, corner flow acts as a volumetrically amplified and highly stable hydrodynamic wetting film. Under the combined effects of nanoparticle adsorption and structural disjoining pressure, capillary condensation preferentially occurs in corner regions. This further enhances the persistence

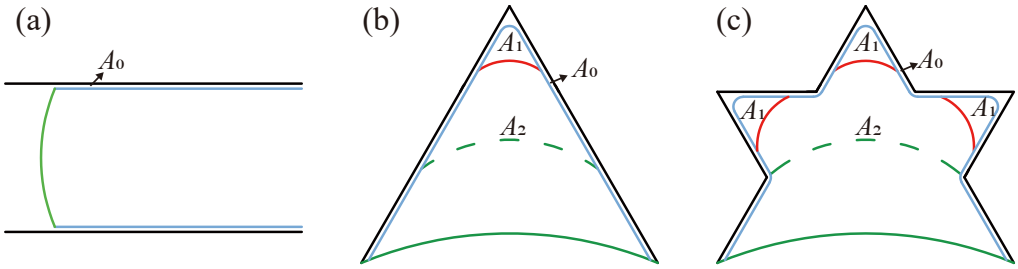

Fig. 6. Illustration of pore filling by NFs within fractal structures: (a)-(c) Different filling stage in the level 0, 1, and 2 fractal structures.

and connectivity of corner flow. The cooperative interaction between corner flow and thin-film flow promotes effective oil mobilization.

In contrast, for SDS surfactant solutions under comparable interfacial tension and wettability conditions, no continuous hydrodynamic wetting film is established (see Lei et al. (2025) for detailed simulations). Curvature-induced capillary effects at microscopic convex features constrain both corner flow and thin-film flow, preventing them from maintaining connectivity. Consequently, their development is suppressed, resulting in significantly lower displacement efficiency compared to NFs.

4.2 Effect of surface roughness

Assuming a connected precursor wetting film along the pore walls, the effect of surface roughness on oil recovery efficiency is further examined. The following experimental conditions and assumptions are specified to highlight the dominant role of pore-scale capillary mechanisms. (i) Oil detachment occurs under quasi-static conditions, such that viscous, inertial, and gravitational forces can be neglected. The corresponding capillary number is $\mathrm{Ca} = \mu U/\sigma \sim 10^{-7}$, and the Bond number is $\mathrm{Bo} = \rho g a^2/\sigma \ll 1$, where μ is the fluid viscosity, U the characteristic velocity, ρ the fluid density, g the gravitational acceleration, and a the characteristic pore size. Under these conditions, the displacement process is governed primarily by capillary pressure and interfacial curvature evolution. (ii) The characteristic scale of random surface roughness introduced during micromachining is several orders of magnitude smaller than that of the designed fractal roughness. Therefore, its influence on interfacial migration is negligible, and the observed behavior is dominated by the designed geometric roughness.

Based on the evolution of interfacial forces during oil detachment within a single roughness element, the process is divided into two sequential stages. Let A denote the area occupied by the aqueous phase within a single roughness element. Here, A_0 represents the area associated with the microscopic roughness corresponding to the thin-film region, while A_1 and A_2 denote the areas of dead-end regions (excluding the microscopic roughness) at different stages, as illustrated in Fig. 6.

(i) Film flow-driven stage ($0 \le A < A_0$)

At this stage, the increase in film thickness originates from capillary condensation within nanoparticle-induced nanostructures. Once a continuous precursor wetting film is established, liquid confined within nanopores formed by adsorbed nanoparticles develops curved menisci. The resulting interfacial pressure gradients drive liquid into the nanoparticle layer. Local condensation further enhances structural disjoining pressure between nanostructures. This promotes progressive film thickening until the region A_0 is fully filled. This stage is therefore governed by disjoining pressure amplification and nanoscale curvature effects, rather than by the designed channel roughness.

(ii) Corner radius-driven stage ($A_0 \le A < A_2$)

When the hydrodynamic wetting film detaches from the microscopic roughness and enters dead-end regions, the governing mechanism shifts. Oil displacement becomes dominated by capillary curvature evolution controlled by corner geometry. During this stage, the corner angle of dead-end pores becomes the key geometric parameter governing meniscus advancement. According to Tuller et al. (1999), the relationship between interfacial curvature and liquid invasion in polygonal corners is expressed analytically. Based on this framework, the curvature radius R_i during the corner flow-dominated stage is given by:

$$R_i = \sqrt{\frac{\sum A_i}{F_n}} \tag{4}$$

where F_n is the geometric angle factor with $F_n = n\tan(\pi/n) - \pi - \sum_{i=1}^{n}[1/\tan(\alpha/2) - (\pi-\alpha)/2]$. For equilateral triangular pores, $\alpha = \pi/3$, $n = 3$, and $F_n = 2.1$.

Once a connected precursor wetting film is established across both primary and secondary structures, the displacement efficiencies are comparable during the film-driven stage. The primary differences among fractal structures arise during the corner radius-controlled stage.

When the wetting phase fills the region A_1, the corner-driven capillary forces associated with the primary and secondary structures are theoretically identical, with $R_1 = \sqrt{A_1/F_n} = 22.70$ μm.

However, compared with the primary structure, the secondary structure introduces additional microscopic roughness units (Fig. 7), significantly enhancing pore-scale curvature heterogeneity. Driven by the connected precursor wetting film, this geometric complexity amplifies the capillary pressure gradient along the wall. As a result, multiple rough substructures are filled simultaneously. Consequently, within the region A_1, the level 2 fractal structure exhibits a faster pore-filling rate over the same time period.

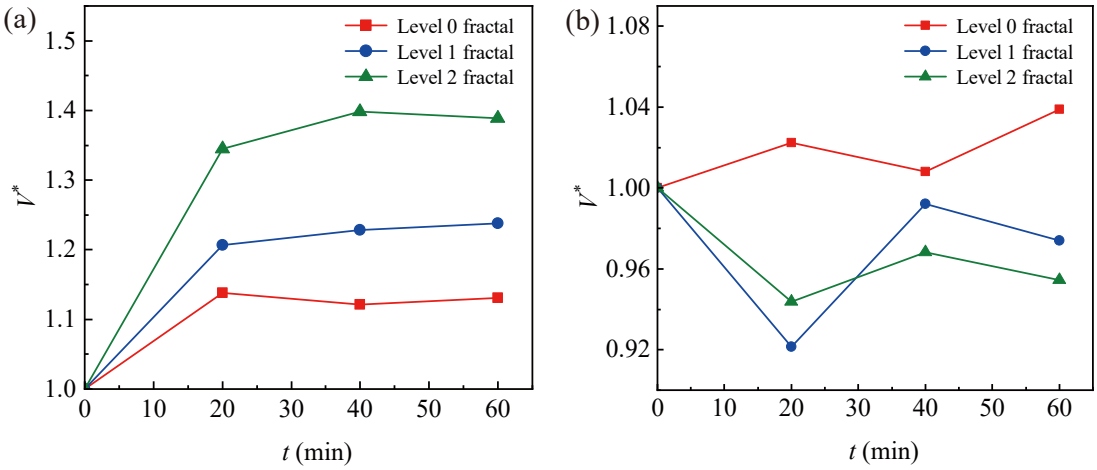

Fig. 7. Normalized SI volume evolution of NFs and SDS solution in micromodels with different fractal structures. (a) NFs and (b) SDS surfactant solutions.

Table 1. Normalized oil displacement volumes within 1 h.

Displacing fluid	Level 0 fractal	Level 1 fractal	Level 2 fractal
NFs	1.13	1.24	1.39
SDS surfactant solutions	1.04	0.97	0.95

Once the wetting phase enters the region A_2, the displacement efficiencies of the level 1 and level 2 fractal structures become nearly identical. Under capillary-dominated conditions, the interface ultimately stabilizes at an angle of approximately 16° relative to the wall, as indicated by the green curve in Fig. 6.

It should be noted that the above analysis of the pore-filling process does not explicitly account for spatial variations in the initial film thickness along the wall surface. In practice, such variations may lead to minor differences in filling rates among microscopic roughness units. For instance, in the level 2 fractal structure, the left rough unit is often filled earlier than adjacent units. However, as the experiments are conducted under quasi-static conditions, these local differences have a negligible effect on the overall displacement behavior.

The transition from disjoining pressure-dominated film thickening to geometry-controlled corner filling establishes a multiscale capillary regulation framework, which explains the superior displacement efficiency of higher-order fractal roughness under SI assisted by NFs.

4.3 Quantification of oil recovery

During SI, mass conservation is maintained within the micromodel. The liquid volume associated with thin-film flow is negligible compared to that of corner flow. Therefore, the cumulative volume contributed by corner flow at a given time can be approximated by the volume of oil displaced, inferred from the recession of the main meniscus (Wijnhorst et al., 2020; Cai et al., 2022; Kubochkin and Gambaryan-Roisman, 2022). Based on this approximation, the oil displacement efficiency under different surface roughness conditions is quantified using the recession volume of the main interface.

Under quasi-static conditions, the cumulative volume of corner flow at time t can be expressed as (Zhang et al., 2021; Zhao et al., 2021):

$$V_t = -aC\sqrt{\frac{2\sigma r^5 t}{k\mu\beta}} \tag{5}$$

where V_t is the cumulative corner flow volume at time t, C is the geometric shape factor, which depends on contact angle and the number of corners, β is the dimensionless flow resistance coefficient, k is a variational parameter obtained by minimizing the deviation between exact and approximate solutions, a is a dimensionless parameter associated with the test function, and r is the characteristic curvature radius of the corner. For a rectangular capillary, which is equivalent to a four-corner geometry, the expression for C can be written as:

$$C = 4\left[\frac{\cos\theta\cos(\pi/4+\theta)}{\sin\pi/4} - (\frac{\pi}{4}-\theta)\right] \tag{6}$$

with $\beta = 99.5$, $k = 1.447$, and $a = 0.59$.

Based on the above model, the theoretical corner flow volumes V_{theory} were first calculated. The theoretical values are 2.52 nL for the NF system and 1.54 nL for the SDS surfactant system. This difference primarily arises from variations in contact angle, as a smaller contact angle leads to a larger theoretical corner flow contribution.

Subsequently, the actual oil displacement volumes under different fractal structures were obtained by quantifying the recession area of the main interface from the experimental images. To enable a meaningful comparison and minimize bias from wettability differences, the measured volumes were normalized by their corresponding theoretical values, defined as $V^* = V_{exp}/V_{theory}$. The normalized results are summarized in Table 1.

Based on the normalized results in Table 1, the temporal evolution of the normalized SI volume is further illustrated in Fig. 7. Compared with the smooth straight channel (level 0), fractal roughness significantly enhances the imbibition

performance of NFs. Specifically, the normalized SI volume increases by 23.8% in the level 1 fractal structure and by 38.9% in the level 2 fractal structure relative to the smooth case. In contrast, the SDS system does not exhibit a monotonic increase in displacement efficiency with increasing surface roughness.

For the NF system, these observations are consistent with the mechanisms discussed in Sections 4.2 and 4.3. Increased surface roughness introduces a greater number of microscale concave features, thereby enhancing local interfacial curvature heterogeneity. This promotes capillary condensation of the precursor wetting film and strengthens corner flow within concave regions. Amplified capillary pressure gradients along rough walls drive oil mobilization. During the corner radius-controlled stage, oil trapped in microscale rough structures is continuously released.

By contrast, in the SDS surfactant system, the absence of a stable and connected hydrodynamic water film suppresses the enhancement induced by surface roughness. Although local concave regions promote capillary condensation and corner flow, the increased presence of convex features leads to film rupture and disrupts continuous liquid transport. As a result, the displacement efficiency of the SDS system does not increase systematically with surface roughness. Its behavior is governed by the spatial competition between concave-induced enhancement and convex-induced inhibition.

The present study establishes a multiscale mechanistic framework for SI in rough microchannels mediated by NFs. Quasi-static corner flow theory is integrated with direct visualization experiments to demonstrate that surface roughness does not universally enhance SI efficiency. Instead, its effect is governed by the stability and connectivity of the interfacial aqueous film.

For conventional surfactant solutions, surface roughness introduces competing geometric effects. Concave features locally enhance capillary condensation and promote corner flow, whereas convex asperities disrupt film continuity and hinder long-range liquid transport. Consequently, displacement efficiency does not increase monotonically with fractal roughness, and spontaneous imbibition remains governed by classical capillary-driven corner flow.

In contrast, the NF system exhibits a fundamentally different response to multiscale roughness. Nanoparticles stabilize the interfacial film and enhance structural disjoining pressure, enabling the formation of a continuous hydrodynamic network along rough surfaces. Under these conditions, microscale concave features amplify curvature gradients, strengthen capillary pressure heterogeneity, and sustain coupling between corner flow and thin-film flow. This cooperative mechanism promotes progressive oil detachment from rough cavities and dead-end pores, resulting in a monotonic increase in displacement efficiency with increasing fractal level.

Comparison between theoretical corner flow scaling and experimental recession volumes shows that NF-enhanced SI cannot be fully described by classical capillary models alone. Instead, the displacement process reflects a curvature-regulated transition. This transition evolves from isolated corner flow to a film-connected transport regime mediated by nanoparticle-induced interfacial stabilization.

Overall, this work demonstrates that the effectiveness of surface roughness in promoting SI depends on the interfacial rheological and structural properties of the displacing fluid. The present study elucidates the coupling between multiscale geometry, capillary forces, and nanoparticle-induced film stabilization, providing new insights into the design of functional imbibition fluids for enhanced oil recovery in complex porous media.

5. Conclusions

SI assisted by NFs was systematically investigated using microfluidic models with controlled fractal roughness and revealed a strong dependence of displacement efficiency on pore surface geometry. Under all roughness conditions considered, NFs consistently outperform surfactant solutions, and this advantage becomes increasingly pronounced as surface roughness increases.

At the pore scale, the enhanced displacement behavior arises from the coupling between precursor wetting films and capillary heterogeneity induced by surface roughness. Under strongly water-wet conditions, a precursor wetting film spreads ahead of the advancing interface along the solid surface, establishing a continuous liquid pathway that maintains interfacial connectivity over rough walls. Meanwhile, surface roughness introduces multiscale geometric undulations and spatial variations in interfacial curvature, thereby redistributing capillary pressure and enhancing axial driving forces. This coupling sustains the development of corner flow and film flow, promotes progressive detachment of trapped oil, and enables efficient transport through geometrically complex regions. Consequently, displacement efficiency cannot be fully explained by interfacial tension reduction alone. Instead, it is governed by precursor wetting film stability and its interaction with capillary effects modulated by surface roughness.

Nevertheless, these insights are derived from simplified microfluidic models, and their applicability to more complex porous media remains to be further examined. The present study is limited to fractal geometries that are approximately two-dimensional and to relatively simple fluid systems. It does not consider three-dimensional pore networks, multiscale structural complexity, or multiphysics coupling processes. In realistic reservoir conditions, the interplay between curvature variations and capillary pressure may exhibit stronger multiscale coupling. This may alter the evolution of precursor films and corner flow. Further investigation in three-dimensional porous structures under more representative conditions is therefore required to enable reliable upscaling from the pore-scale to the reservoir-scale.

Despite these limitations, the coupling between precursor wetting films and surface roughness provides a new perspective for understanding interfacial transport in complex porous media. Such insights may also improve understanding of multiphase flow behavior and provide useful guidance for applications such as unconventional hydrocarbon recovery, CO_2 sequestration, and subsurface remediation.

Acknowledgements

The authors acknowledge financial support from the Deep Earth Probe and Mineral Resources Exploration-National Science and Technology Major Project (No. 2024ZD1004502), National Natural Science Foundation of China (Nos. 52274045, 52574129 and 52274104), the Fundamental Research Funds for the Central Universities (No. 2026JCCXMT01), the National Science and Technology Major Project of New Oil and Gas Exploration and Development (No. 2025ZD1406204), and the Newton International Fellowship funded by the Royal Society (W. L).

Conflicts of interest

The authors declare no competing interest.

References

Ajaev, V. S., Gatapova, E. Y., Kabov, O. A. Stability and break-up of thin liquid films on patterned and structured surfaces. Advances in Colloid and Interface Science, 2016, 228: 92-104.

Alvarez-Berrios, M. P., Aponte-reyes, L. M., Aponte-cruz, L. M., et al. Effect of the surface charge of silica nanoparticles on oil recovery: Wettability alteration of sandstone cores and imbibition experiments. International Nano Letters, 2018, 8: 181-188.

Anand, U., Ghosh, T., Aabdin, Z., et al. Dynamics of thin precursor film in wetting of nanopatterned surfaces. Proceedings of the National Academy of Sciences, 2021, 118(38): e2108074118.

Belhaj, A. F., Elraies, K. A., Alnarabiji, M. S., et al. Experimental investigation of surfactant partitioning in pre-CMC and post-CMC regimes for enhanced oil recovery application. Energies, 2019, 12(12): 2319.

Burstein, L. Lubrication and roughness, in Tribology for Engineers, edited by C. M. Taylor, Woodhead Publishing, Cambridge, pp. 65-120, 2011.

Cai, J., Chen, Y., Liu, Y., et al. Capillary imbibition and flow of wetting liquid in irregular capillaries: A 100-year review. Advances in Colloid and Interface Science, 2022, 304: 102654.

Cardona, A., Santamarina, J. C. Immiscible imbibition in fractured media: A dual-porosity microfluidics study. International Journal of Rock Mechanics and Mining Sciences, 2023, 170: 105555.

Furedi, M., Manzano, C. V., Marton, A., et al. Beyond the meso/macroporous boundary: Extending capillary condensation-based pore size characterization in thin films through tailored Adsorptives. The Journal of Physical Chemistry Letters, 2024, 15(5): 1420-1427.

Geistlinger, H., Ataei-Dadavi, I., Mohammadian, S., et al. The impact of pore structure and surface roughness on capillary trapping for 2-D and 3-D porous media: Comparison with percolation theory. Water Resources Research, 2015, 51(11): 9094-9111.

Guo, W., Sun, Y., Luo, G., et al. Interaction of PEG with ionic surfactant SDS to form template for mesoporous material. Colloids and Surfaces A: Physicochemical and Engineering Aspects, 2005, 252(1): 71-77.

Hu, Y., Zhao, C., Zhao, J., et al. Mechanisms of fracturing fluid spontaneous imbibition behavior in shale reservoir: A review. Journal of Natural Gas Science and Engineering, 2020, 82: 103498.

Ichikawa, N., Hosokawa, K., Maeda, R. Interface motion of capillary-driven flow in rectangular microchannel. Journal of Colloid and Interface Science, 2004, 280(1): 155-164.

Jing, Y., Raffa, P., Druetta, P. Recent advances on the numerical modeling and simulation of nanoparticle-assisted CO_2 enhanced oil recovery. Chemical Engineering Journal, 2025, 525: 170396.

Kondiparty, K., Nikolov, A., Wu, S., et al. Wetting and spreading of nanofluids on solid surfaces driven by the structural disjoining pressure: statics analysis and experiments. Langmuir, 2011, 27(7): 3324-3335.

Ko, S., Huh, C. Use of nanoparticles for oil production applications. Journal of Petroleum Science and Engineering, 2019, 172: 97-114.

Kovalchuk, N. M., Trybala, A., Starov, V., et al. Fluoro-vs hydrocarbon surfactants: Why do they differ in wetting performance? Advances in Colloid and Interface Science, 2014, 210: 65-71.

Kubochkin, N., Gambaryan-Roisman, T. Capillary-driven flow in corner geometries. Current Opinion in Colloid & Interface Science, 2022, 59: 101575.

Lei, W., Gong, W., Lu, X., et al. Fluid entrapment during forced imbibition in a multidepth microfluidic chip with complex porous geometry. Journal of Fluid Mechanics, 2024, 987: A3.

Lei, W., Liu, T., Xie, C., et al. Enhanced oil recovery mechanism and recovery performance of micro-gel particle suspensions by microfluidic experiments. Energy Science & Engineering, 2020, 8(4): 986-998.

Lei, W., Lu, X., Wang, M. Multiphase displacement manipulated by micro/nanoparticle suspensions in porous media via microfluidic experiments: From interface science to multiphase flow patterns. Advances in Colloid and Interface Science, 2023, 311: 102826.

Lei, W., Lu, X., Yang, G., et al. Reverse capillary trapping and self-removal of non-aqueous fluid from dead-end structures by nanoparticle suspension. Journal of Fluid Mechanics, 2025, 1009: A14.

Li, C., Yu, C., Zhou, S., et al. Liquid harvesting and transport on multiscaled curvatures. Proceedings of the National Academy of Sciences, 2020, 117(38): 23436-23442.

Lim, S., Zhang, H., Wu, P., et al. The dynamic spreading of nanofluids on solid surfaces–role of the nanofilm structural disjoining pressure. Journal of Colloid and Interface Science, 2016, 470: 22-30.

Lu, X., Zhang, M., Lei, W., et al. Spreading versus non-spreading of wetting films: Enhancing aqueous phase invasion in disordered media via nanoparticle adsorption.

Journal of Fluid Mechanics, 2026, 1030: R5.

Matar, O. K., Craster, R. V., Sefiane, K. Dynamic spreading of droplets containing nanoparticles. Physical Review E – Statistical, Nonlinear, and Soft Matter Physics, 2007, 76(5): 056315.

MacDowell, L. G., Benet, J., Katcho, N. A., et al. Disjoining pressure and the film-height-dependent surface tension of thin liquid films: New insight from capillary wave fluctuations. Advances in Colloid and Interface Science, 2014, 206: 150-171.

Murshed, S. M., Nieto de Castro, C. A. Spreading characteristics of nanofluid droplets impacting onto a solid surface. Journal of Nanoscience and Nanotechnology, 2011, 11(4): 3427-3433.

Nguele, R., Sreu, T., Inoue, H., et al. Enhancing oil production using silica-based nanofluids: Preparation, stability, and displacement mechanisms. Industrial & Engineering Chemistry Research, 2019, 58(32): 15045-15060.

Nikolov, A., Wu, P., Wasan, D. Structure and stability of nanofluid films wetting solids: An overview. Advances in Colloid and Interface Science, 2019, 264: 1-10.

Panter, J. R., Konicek, A. R., King, M. A., et al. Rough capillary rise. Communications Physics, 2023, 6(1): 44.

Robbins, M. O., Andelman, D., Joanny, J. F. Thin liquid films on rough or heterogeneous solids. Physical Review A, 1991, 43(8): 4344.

Ratanpara, A., Kim, M. Wettability alteration mechanisms in enhanced oil recovery with surfactants and nanofluids: A review with microfluidic applications. Energies, 2023, 16(24): 8003.

Ruiz-Gutiérrez, É., Armstrong, S., Lévêque, S., et al. The long cross-over dynamics of capillary imbibition. Journal of Fluid Mechanics, 2022, 939: A39.

Sekoai, P. T., Ouma, C. N. M., Du Preez, S. P., et al. Application of nanoparticles in biofuels: An overview. Fuel, 2019, 237: 380-397.

Song, W., de Haas, T. W., Fadaei, H., et al. Chip-off-the-old-rock: The study of reservoir-relevant geological processes with real-rock micromodels. Lab on a Chip, 2014, 14(22): 4382-4390.

Tavakkoli, O., Kamyab, H., Junin, R., et al. SDS-aluminum oxide nanofluid for enhanced oil recovery: IFT, adsorption, and oil displacement efficiency. ACS Omega, 2022, 7(16): 14022-14030.

Tian, W., Wu, K., Gao, Y., et al. A critical review of enhanced oil recovery by imbibition: Theory and practice. Energy & Fuels, 2021, 35(7): 5643-5670.

Tuller, M., Or, D., Dudley, L. M. Adsorption and capillary condensation in porous media: Liquid retention and interfacial configurations in angular pores. Water Resources Research, 1999, 35(7): 1949-1964.

Thiele, U., Goyeau, B., Velarde, M. G. Stability analysis of thin film flow along a heated porous wall. Physics of Fluids, 2009, 21(1): 014103.

Wang, K., You, Q., Long, Q. M., et al. Experimental study of the mechanism of nanofluid in enhancing the oil recovery in low permeability reservoirs using microfluidics. Petroleum Science, 2023, 20(1): 382-395.

Whitesides, G. M. The origins and the future of microfluidics. Nature, 2006, 442(7101): 368-373.

Wijnhorst, R., de Goede, T. C., Bonn, D., et al. Surfactant effects on the dynamics of capillary rise and finger formation in square capillaries. Langmuir, 2020, 36(46): 13784-13792.

Xu, W., Song, Y., Xu, R., et al. Electrohydrodynamic and hydroelectric effects at the water-solid interface: From fundamentals to applications. Advanced Materials Interfaces, 2021, 8(2): 2000670.

Yarveicy, H. Effect of nanoparticles on phase behavior of surfactant-oil-water system: An application in multiphase flow system. Advances in Geo-Energy Research, 2023, 9(3): 152-155.

Yekeen, N., Padmanabhan, E., Idris, A. K., et al. Nanoparticles applications for hydraulic fracturing of unconventional reservoirs: A comprehensive review of recent advances and prospects. Journal of Petroleum Science and Engineering, 2019, 178: 41-73.

Youssif, M. I., El-Maghraby, R. M., Saleh, S. M., et al. Silica nanofluid flooding for enhanced oil recovery in sandstone rocks. Egyptian Journal of Petroleum, 2018, 27(1): 105-110.

Zhang, J., Zhang, H., Lee, D., et al. Microfluidic study on the two-phase fluid flow in porous media during repetitive drainage-imbibition cycles and implications to the CAES Operation. Transport in Porous Media, 2020, 131(2): 449-472.

Zhang, Y., Liu, B., Jia, X., et al. Comparison of nanofluid wetting characteristics in untreated and superhydrophilic microgrooved heat pipes. Case Studies in Thermal Engineering, 2021, 25: 100956.

Zhang, H., Ramakrishnan, T. S., Nikolov, A., et al. Enhanced oil displacement by nanofluid's structural disjoining pressure in model fractured porous media. Journal of Colloid and Interface Science, 2018, 511: 48-56.

Zhao, J., Qin, F., Fischer, R., et al. Spontaneous imbibition in a square tube with corner films: Theoretical model and numerical simulation. Water Resources Research, 2021, 57(2): e2020WR029190.

Zhao, J., Qin, F., Fei, L., et al. Competition between main meniscus and corner film flow during imbibition in a strongly wetting square tube. Journal of Hydrology, 2022, 615: 128695.

Zheng, J., Qi, X., Gong, W., et al. Investigating snap-off behavior during spontaneous imbibition in 3D pore-throat model by pseudopotential lattice Boltzmann method. Advances in Water Resources, 2024, 190: 104751.